Capacity of the Watermark-Channel: How Many Bits Can Be Hidden Within a Digital Image ?

M.Barni[a], F.Bartolini[b], A. De Rosa[b], and A.Piva[b]

[a]Department of Information Engineering, University of Siena
Via Roma 56, 53100 - Siena, Italy
e-mail: barni@dii.unisi.it

[b]Department of Electronic Engineering, University of Florence
Via di Santa Marta 3, 50139 - Florence, Italy
e-mail: {barto piva derosa}@lci.die.unifi.it

ABSTRACT

An evaluation of the number of bits that can be hidden within an image by means of frequency-domain watermarking is given. Watermarking is assumed to consist in the modification of a set of full-frame DCT (DFT) coefficients. The amount of modification each coefficient undergoes is proportional to the magnitude of the coefficient itself, so that an additive-multiplicative embedding rule results. The watermark-channel is modeled by letting the watermark be the signal and the image coefficients the noise introduced by the channel. To derive the capacity of each coefficient, the input (i.e. the watermark) and the output (i.e. the watermarked coefficients) of the channel are quantized, thus leading to a discrete-input, discrete-output model. Capacity is evaluated by computing the channel transition matrix and by maximizing the mutual input/output information. Though the results we obtained do not take into account attacks, they represent a useful indication about the amount of information that can be hidden within a single image

Keywords: Digital watermarking, image watermarking, frequency-domain watermarking, watermark capacity, copyright protection, DCT/DFT coefficient modeling

1. INTRODUCTION

Though the introduction of digital watermarking as a tool for copyright protection is quite recent, a great deal of research has been carried out mainly addressing the development of robust, yet unperceivable, watermarking strategies.[1] As it is now becoming evident, however, other important issues have to be analyzed in order to make watermark-based copyright protection feasible.[2–4] Among them, the evaluation of the maximum number of information bits that can be hidden within a piece of data of a given size plays a mayor role.

Existing works addressing this problem model the watermarking process as a communication task, consisting of two main steps: *watermark casting*, in which the signal, namely the watermark, is transmitted over the channel (hereafter the watermark-channel) that the to-be-marked-data acts the part of, and *watermark detection*, in which the signal is received and extracted from data. According to Smith and Comiskey[5] and Servetto et al.[6] , the watermark-channel is modeled as an AWGN channel, so that the corresponding popular capacity theorem[7] can be used. Such an analysis, however, only applies to cases where the watermark is simply added to a set of features extracted from the host data. Besides, the features the watermark is added to, must be such that they can be modeled as Gaussian random variables. As a matter of fact, the embedding rule is only rarely additive, and the Gaussian approximation is not verified in most practical cases. In addition, attacks, be they malicious or not, are not considered at all by such an oversimplified model. Further research is then needed to establish an upper limit to the number of bits which can be conveyed by any single piece of data.

In this work the evaluation of the number of bits which can be hidden within an image by means of a class of image watermarking algorithms operating in the frequency domain is addressed. According to the approaches proposed by Cox et al.[8] , and Barni et al.[9] , watermark embedding is achieved by modifying a set of full-frame DCT coefficients of the image. Alternatively, the magnitude of the DFT coefficients may be modified to achieve translation invariance[10,11] . In any case, the amount of modification each coefficient undergoes is proportional to the magnitude of the coefficient itself as expressed by the following rule:

$$y_i = x_i + \gamma m_i |x_i| \tag{1}$$

Part of the IS&T/SPIE Conference on Security and Watermarking of Multimedia Contents
San Jose, California • January 1999
SPIE Vol. 3657 • 0277-786X/99/$10.00

where x_i indicates the original DCT coefficient, y_i the marked coefficient, m_i the i-th component of the watermark, i accounts for the position of the marked coefficient within the frequency spectrum, and γ is a parameter controlling the watermark strength. In the case of DFT watermarking, equation (1) is rewritten as:

$$y_i = x_i + \gamma m_i x_i \tag{2}$$

where x_i denotes the magnitude of the i-th DFT coefficient, and y_i the corresponding marked magnitude. To simplify the analysis, we will assume that m_i's take values in a finite interval, say $[-1, 1]$. This does not preclude the generality of our results, since in practical applications watermark coefficients are always limited. Besides, as it has been shown by Kalker et al.[12] , the probability distribution of the watermark coefficients does not have a significant impact on watermark decoding reliability. By following the communication paradigm outlined previously, we can assimilate the i-th component of the watermark m_i to the to-be-transmitted signal, the i-th marked coefficient y_i to the channel output, and the i-th non-marked DCT/DFT coefficient x_i to channel noise. It is evident that, even by neglecting the presence of attacks, the additive Gaussian noise assumption does not hold. Indeed the noise is additive-multiplicative and does not follow a Gaussian probability density function (pdf), since neither DCT nor DFT coefficients can be modeled as Gaussian random variables.

In the next sections, a numerical methodology will be described, which permits to evaluate the capacity of the watermark-channel as defined by equations (1) and (2). The proposed methodology will then be used to evaluate the number of bits that can be hidden in some test images.

2. WATERMARK-CHANNEL MODELING

Let $f_{m_i}(m)$ and $f_{x_i}(x)$ denote the pdf of the i-th random variables m_i and x_i respectively (hereafter the index i will be overlooked since we will assume that m_i's and x_i's are independent identically distributed, iid, variables). By relying on equations (1) and (2), the pdf $f_y(y)$ of the marked coefficient y subject to a watermark value m can be written as

$$f_y(y|m) = \frac{1}{1+\gamma\ m\ sign(y)} f_x\left(\frac{y}{1+\gamma\ m\ sign(y)}\right) \tag{3}$$

in the DCT case, and

$$f_y(y|m) = \frac{1}{1+\gamma\ m} f_x\left(\frac{y}{1+\gamma\ m}\right) \tag{4}$$

in the case the watermark is embedded in the DFT domain. Note that equation (3) includes equation (4) as a special case, since when y represents the magnitude of DFT coefficients, $sign(y)$ is always equal to $+1$.

According to the approach proposed here, to derive the channel capacity $\mathcal{C}_W$ for each use of the channel, i.e. the capacity of each DCT (DFT) coefficient, both the input m and the output y of the channel are quantized, thus leading to a discrete-input, discrete-output model. By assuming DCT (DFT) coefficients are independent each other, and by noting that m's are iid random variables, we can conclude that the watermark-channel is a memoryless one.

Once the input (output) quantization values have been fixed, the channel is completely described by the input alphabet $\mathcal{M} = \{\hat{m}_0, \hat{m}_1, \ldots \hat{m}_{K-1}\}$, the output alphabet $\mathcal{Y} = \{\hat{y}_0, \hat{y}_1, \ldots \hat{y}_{J-1}\}$ and the set of transition probabilities $\{p(\hat{y}_j|\hat{m}_k),\ j = 0, 1 \ldots J-1,\ k = 0, 1 \ldots K-1\}$, where $\hat{m}_i$ and $\hat{y}_i$ indicate the i-th input and output quantized values respectively. Transition probabilities can be calculated by integrating the conditional pdf in equations (3) and (4), which yields:

$$p(\hat{y}_j|\hat{m}_k) = \int_{\hat{y}_j}^{\hat{y}_{j+1}} f_y(y|\hat{m}_k)dy. \tag{5}$$

Given the channel transition matrix $\mathbf{P} = \{p(\hat{y}_j|\hat{m}_k)\}_{k,j}$, and the a-priori probabilities $p(\hat{m}_i)$, the mutual information of the channel is defined by the equation:

$$I(\mathcal{M};\mathcal{Y}) = \sum_{j,k} p(\hat{m}_k)p(\hat{y}_j|\hat{m}_k) \log\left[\frac{p(\hat{y}_j|\hat{m}_k)}{\sum_i p(\hat{m}_i)p(\hat{y}_j|\hat{m}_i)}\right], \tag{6}$$

whose maximization over all possible sets of input probabilities gives the capacity for each single use of the channel, i.e. the capacity of each DCT (DFT) coefficient. To calculate the maximum of $I(\mathcal{M};\mathcal{Y})$, let us recall that the mutual information of a discrete memoryless channel is a convex function of $p(\mathcal{M}) = \{p(\hat{m}_0), p(\hat{m}_1), \ldots p(\hat{m}_{K-1})\}$[13] . The watermark-channel capacity C_W, then, can be obtained numerically by maximizing $I(\mathcal{M};\mathcal{Y})$ over the K variables $\{p(\hat{m}_k)\}$, subject to the constraints:

$$p(\hat{m}_k) \geq 0 \quad \forall k \tag{7}$$

$$\sum_{k=0}^{K-1} p(\hat{m}_k) = 1. \tag{8}$$

The estimation of the probability density function of DCT (DFT) coefficients, that is needed to actually evaluate C_W, is addressed in sections 3 and 4 respectively.

3. STATISTICAL MODELING OF DCT COEFFICIENTS

As it has been suggested by Müller,[14] Joshi and Fischer[15] , and Barni et al.[16] , we will assume that full-frame DCT coefficients follow a zero-mean Generalized Gaussian pdf, defined as:

$$f_{GG}(x) = \frac{\nu\alpha(\nu)}{2\sigma\Gamma(1/\nu)} \exp\left[-\left(\frac{\alpha(\nu)}{\sigma}|x|\right)^{\nu}\right], \tag{9}$$

where

$$\alpha(\nu) = \sqrt{\frac{\Gamma(3/\nu)}{\Gamma(1/\nu)}}, \tag{10}$$

and $\Gamma(\cdot)$ denotes the usual gamma function

$$\Gamma(\delta) = \int_0^{\infty} x^{\delta-1} e^{-x} dx. \tag{11}$$

With regard to ν and σ, they are real valued positive constants, controlling the pdf shape and variance respectively. More specifically, when $\nu = 1$, the Generalized Gaussian reduces to a Laplacian distribution, whereas by letting $\nu = 2$, a Gaussian pdf is obtained. The shape of the $f_{GG}(x)$ for various shape parameters is depicted in figure 1. By replacing $f_x(x)$ with $f_{GG}(x)$ in equation (3), $f_y(y|m)$ can be given the form:

$$f_y(y|m) = \frac{1}{1+\gamma\ m\ sign(y)} \cdot \frac{\nu\alpha(\nu)}{2\sigma\Gamma(1/\nu)} \exp\left[-\left(\frac{\alpha(\nu)}{\sigma}\left|\frac{y}{1+\gamma\ m\ sign(y)}\right|\right)^{\nu}\right] \tag{12}$$

Inserting equation (12) in the expression of the channel transition matrix yields:

$$p(\hat{y}_j|\hat{m}_k) = \int_{\hat{y}_j}^{\hat{y}_{j+1}} f_y(y|\hat{m}_k)dy = \int_{\hat{y}_j}^{\hat{y}_{j+1}} \frac{1}{1+\gamma\ \hat{m}_k\ sign(y)} \frac{\nu\alpha(\nu)}{2\sigma\Gamma(1/\nu)} \exp\left[-\left(\frac{\alpha(\nu)}{\sigma}\left|\frac{y}{1+\gamma\ \hat{m}_k\ sign(y)}\right|\right)^{\nu}\right] dy \tag{13}$$

Finally, to actually derive the watermark-channel capacity, the integrals in equation (13) must be evaluated numerically and the results fed into the maximization process.

4. STATISTICAL MODELING OF DFT COEFFICIENTS

When the watermark is inserted in the magnitude of the DFT spectrum, the analysis carried out in section 3 no longer holds, since the Generalized Gaussian distribution is not suited to describe positive-valued random variables, such as DFT coefficients are. What is needed here is a parametric pdf which is defined on the positive real axis only, and which is both flexible and easy to handle from a mathematical point of view. As for the Generalized Gaussian

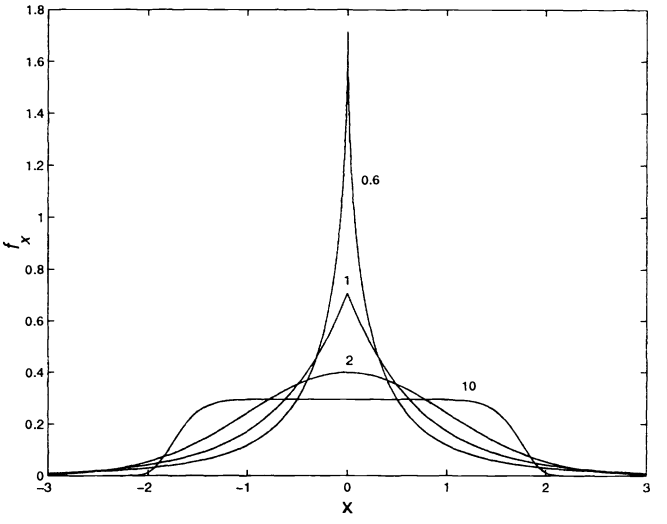

Figure 1. Shape of the Generalized Gaussian distribution for various ν. The effect of varying ν on the pdf shape can be appreciated.

case, parametrization should permit the description of random variables characterized by pdf's with different variance and shape. A possible solution is to describe the DFT coefficients through the Weibull distribution, defined as:

$$f_W(x) = \frac{\beta}{\alpha}\left(\frac{x}{\alpha}\right)^{\beta-1} \exp\left[-\left(\frac{x}{\alpha}\right)^{\beta}\right], \tag{14}$$

where $\alpha > 0$ and $\beta > 0$ are real-valued positive constants controlling the pdf mean, variance and shape. In particular, the mean and variance of the Weibull pdf can be expressed as follows:

$$\mu_x = \alpha\Gamma\left(1+\frac{1}{\beta}\right) \tag{15}$$

and variance:

$$\sigma_x^2 = \alpha^2\left\{\Gamma\left(1+\frac{2}{\beta}\right) - \left[\Gamma\left(1+\frac{1}{\beta}\right)\right]^2\right\} = \alpha^2\Gamma\left(1+\frac{2}{\beta}\right) - \mu_x^2, \tag{16}$$

Limit cases are obtained by letting β =1 and $\beta = 2$, when an exponential and a Rayleigh distribution are obtained respectively. The shape of some Weibull probability density functions with different values of the parameters α and β are reported in figures 2 through 4. By inserting equation (14) in equation (4), the pdf of marked DFT coefficients is achieved

$$f_y(y|m) = \frac{\beta}{\alpha(1+\gamma m)}\left(\frac{y}{\alpha(1+\gamma m)}\right)^{\beta-1} \exp\left[-\left(\frac{y}{\alpha(1+\gamma m)}\right)^{\beta}\right] \tag{17}$$

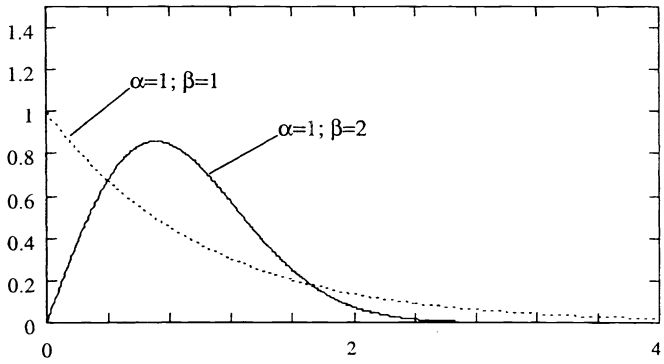

Figure 2. For $\beta = 1$ the Weibull pdf degenerates into an exponential pdf, whereas by letting $\beta = 2$ a Rayleigh probability density function is obtained.

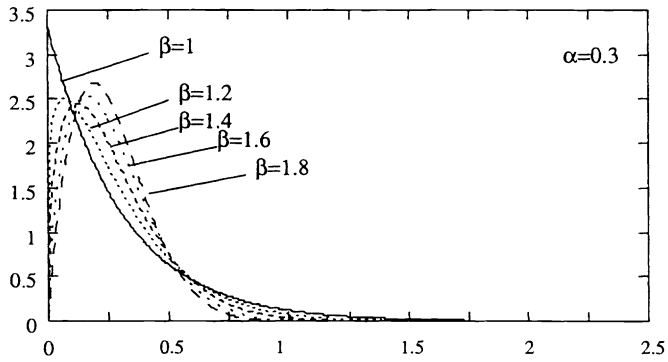

Figure 3. Effect of varying β on the shape of the Weibull probability density function.

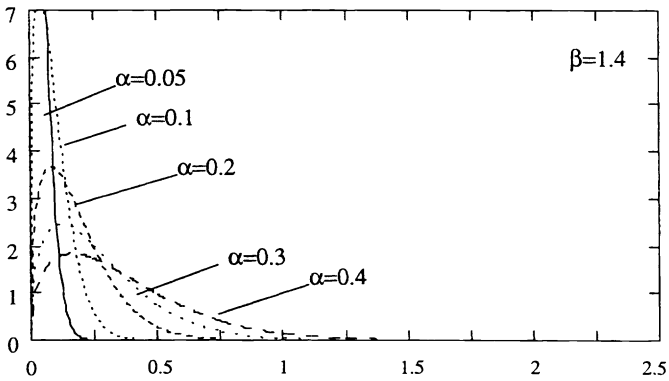

Figure 4. In the diagram the dependence of the shape of the Weibull distribution upon the parameter α is highlighted.

The channel transition matrix $\mathbf{P} = \{p(\hat{y}_j|\hat{m}_k)\}_{k,j}$ is obtained by integrating $f_y(y|\hat{m}_k)$ over each output quantization interval:

$$p(\hat{y}_j|\hat{m}_k) = \int_{\hat{y}_j}^{\hat{y}_{j+1}} \frac{\beta}{\alpha(1+\gamma\hat{m}_k)} \left(\frac{y}{\alpha(1+\gamma\hat{m}_k)}\right)^{\beta-1} \exp\left[-\left(\frac{y}{\alpha(1+\gamma\hat{m}_k)}\right)^{\beta}\right] dy \tag{18}$$

$$= -\exp\left[-\left(\frac{y}{\alpha(1+\gamma\hat{m}_k)}\right)^{\beta}\right]\Bigg|_{\hat{y}_j}^{\hat{y}_{j+1}}$$

$$= -\exp\left[-\left(\frac{\hat{y}_{j+1}}{\alpha(1+\gamma\hat{m}_k)}\right)^{\beta}\right] + \exp\left[-\left(\frac{\hat{y}_j}{\alpha(1+\gamma\hat{m}_k)}\right)^{\beta}\right].$$

As opposed to the Generalized Gaussian (DCT) case, the elements of the transition matrix $\mathbf{P}$ can be evaluated exactly. Such values are used to maximize the mutual information of the channel, eventually yielding the watermark-channel capacity for each marked DFT coefficient.

5. RESULTS ON TEST DATA

To apply the analysis carried out so far to the actual estimation of $\mathcal{C}_W$, some parameters have to be fixed: the range of the output random variable y, the input (output) quantization step, and the value of γ; in addition, the parameters describing the DCT (DFT) coefficients pdf have to be estimated.

Theoretically, the range of values watermarked coefficients can assume is infinite; however, if values occurring with probability lower than say 10^{-3} are neglected, the following relation holds

$$p(y \in (-\infty, \hat{y}_0] \cup [\hat{y}_{J-1}, +\infty)) = \int_{-\infty}^{\hat{y}_0} f_y(y)dy \; + \; \int_{\hat{y}_{J-1}}^{+\infty} f_y(y)dy \; < 10^{-3}. \tag{19}$$

If y_{DCT} denotes the channel output in the case the watermark is inserted in the DCT domain, by evaluating the integrals in equation (19), it can be shown that $y_{DCT} \in [-4; 4]$ represent a reasonable choice. By proceeding in the same way, it is also found that $y_{DFT} \in [0; 0.4]$ is a good approximation, where y_{DFT} is the analogous of y_{DCT} in the DFT case.

To choose the input (output) quantization step Δm (Δy), the computation of the channel capacity was repeated iteratively each time decreasing the quantization steps, until the capacity converged to a finite value. It is such a final value that is assumed to represent the channel capacity for the continuous case. By operating in this way, we found that good results are obtained by letting $\Delta m_{DCT} = \Delta m_{DFT} = 0.1$, $\Delta y_{DCT} = 0.02$ and $\Delta y_{DFT} = 0.001$, where the subscripts DCT and DFT have been added to distinguish between the techniques operating in the DCT domain and those embedding the watermark in the DFT domain. As to γ, in the first instance, it was set to 0.2.

In figure 5, the capacity $\mathcal{C}_W$ of a channel characterized by coefficients having a Generalized Gaussian distribution is plotted for several values of the parameters ν and σ. As a first evidence, it comes out that the capacity increases with the shape parameter ν. Besides, $\mathcal{C}_W$ decreases as the coefficient variance increases. This is not surprising if we remember that in the watermark-channel model the image coefficients represent noise, and that, of course, the higher the noise the lower the capacity. Note also that when the variance gets lower and lower a region is found where $\mathcal{C}_W$ is nearly constant. For even smaller values of σ, the capacity starts decreasing again. Results obtained with very small variance, however, are not much significant, since in such a case both the signal and channel noise tend to zero. The results depicted in figure 5 conflict with the common-sense intuition that images with strong activity, i.e. large coefficient variance, can bear more information bits. This apparent contradiction can be explained by noting that the amount of information that can be hidden within an image also depends on the watermark energy, which, in turn, can assume higher values in images characterized by higher variance, where watermark invisibility is more easily achieved. To account for the dependence of $\mathcal{C}_W$ upon the watermark strength γ, some tests have been carried out by fixing ν and σ, and varying γ. The results we obtained are reported in figures 6 through 8. As it was expected, the dependence of $\mathcal{C}_W$ on γ is confirmed, in that a higher energy ensures a higher capacity. To move the analysis one step further, one would need to know the dependence of γ upon the image coefficients variance. Stated in another

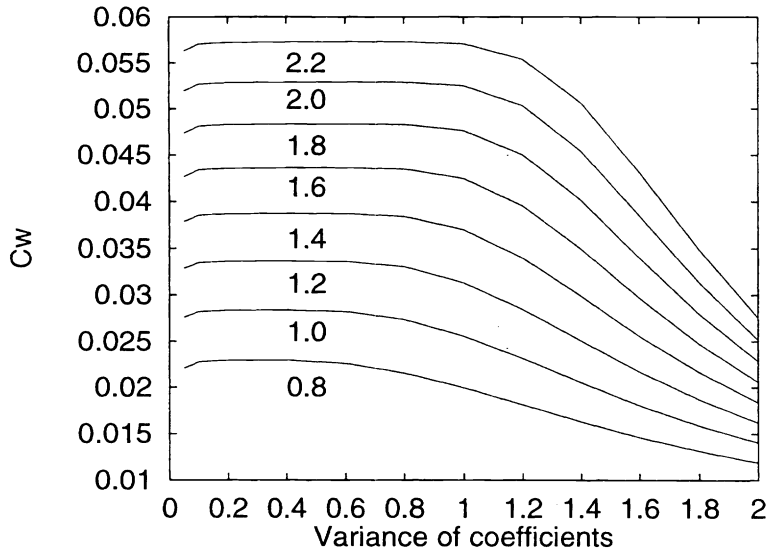

Figure 5. Watermark-channel capacity for the case of Gaussian coefficients. The capacity is plotted for shape parameters ranging from 0.8 through 2.2.

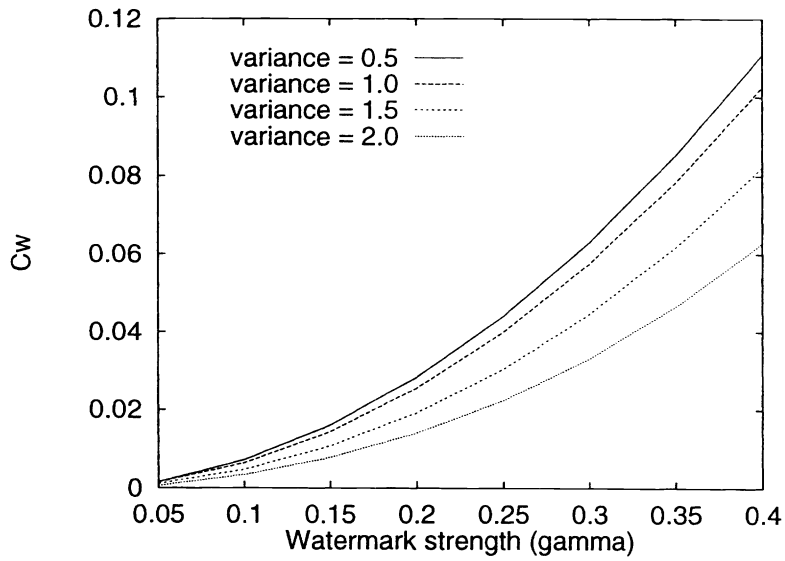

Figure 6. Dependence of C_W on watermark strength γ. The shape parameter ν was set to 1.0. Four curves are plotted referring to coefficients characterized by different variance.

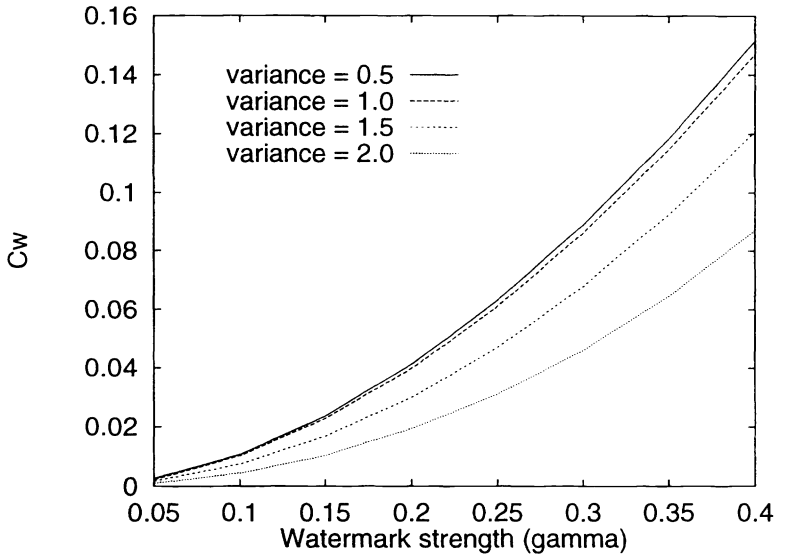

Figure 7. Dependence of C_W on watermark strength γ. The shape parameter ν was set to 1.5. Four curves are plotted referring to coefficients characterized by different variance.

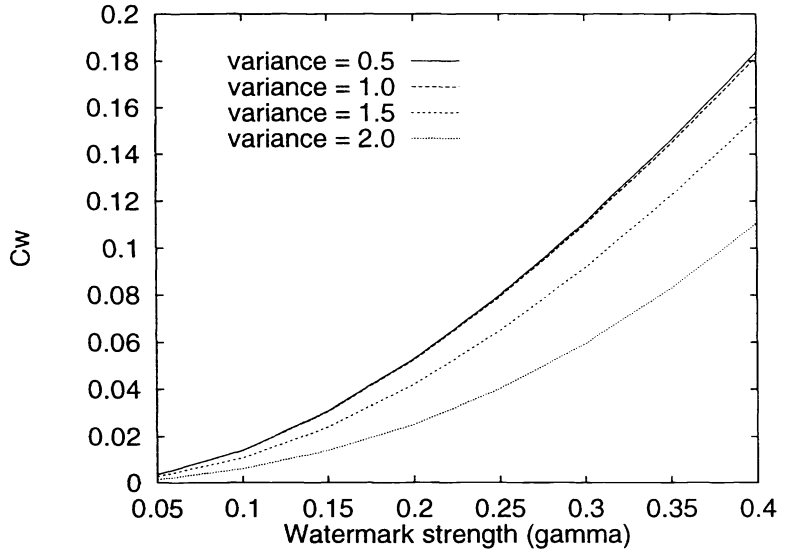

Figure 8. Dependence of C_W on watermark strength γ. The shape parameter ν was set to 2.0. Four curves are plotted referring to coefficients characterized by different variance.

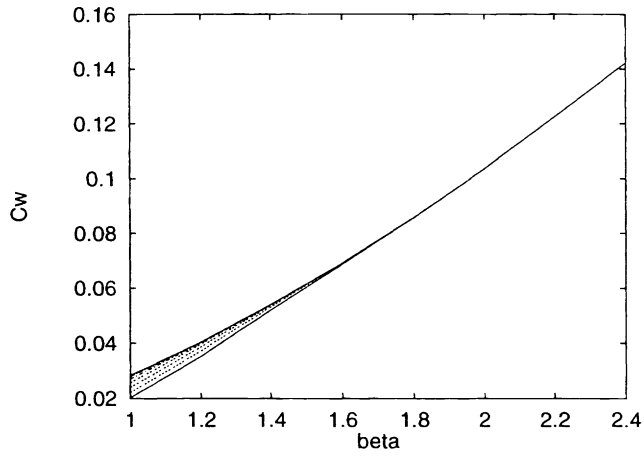

Figure 9. Watermark-channel capacity for the case of Weibull-distributed coefficients. In the diagram β ranges from 1.0 through 2.4. Ten curves are plotted for $\alpha = 0.01, 0.02...0.1$. Curves with lower capacity correspond to higher values of α.

way, the maximum watermark energy allowed for an image characterized by a given variance under the constraint of watermark invisibility, should be evaluated. Unfortunately, it is not easy to model the above dependence, hence we will not consider the problem any further.

An analysis similar to that carried out for Gaussian coefficients was performed for the Weibull channel case. The results we obtained are reported in figure 9, where $\mathcal{C}_W$ is plotted for different values of the parameters α and β ($\alpha \in [0.01, 0.1], \beta = [1.0, 2.4]$). It is noteworthy that the values of α and β used in the figure have been chosen since they are representative of the values encountered in real world imagery (see below in the text). At a first glance the results reported in figure 9 may appear quite strange, since they suggest that $\mathcal{C}_W$ does not depend on α, which should not be the case, since the value of α is directly related to the coefficients variance (see eq. (16)). However, by observing the diagrams reported in figure 5 and by inserting in equation (16) the values of α and β used here, this apparent contradiction is easily explained. As a matter of fact, by letting α and β vary in the intervals $[0.01, 0.1]$ and $[1.0, 2.4]$ respectively, we are positioning our experiments in the flat portion of the $\sigma - \mathcal{C}_W$ diagram, hence it is not surprising that $\mathcal{C}_W$ does not depend on α, i.e. the variance of the coefficients.

It is also interesting to compare the results obtained in the DFT and DCT cases. As it can be seen, a higher capacity results in the former case, however this does not mean that by embedding the watermark in the DFT domain a higher capacity can be achieved, since to ultimately decide which domain ensures a higher capacity, the visibility of the watermark should be taken into account as well.

In addition to the tests described above, experiments on some standard 512×512 real world images were carried out. For each image, both DCT and DFT watermark embedding have been considered. In figure 10a the region of the DCT spectrum the watermark is embedded in is depicted. Such a region was split into 16 smaller sub-regions. According to the approach we followed throughout the experiments, the coefficients of each sub-region are assumed to have the same pdf. The parameters ν and σ characterizing the coefficients of each sub-region were then evaluated by applying the Maximum Likelihood criterion to the DCT samples contained in it. Finally, the estimated parameters were used to evaluated the watermark-channel capacity $\mathcal{C}_i$ per each DCT coefficient, where i denotes which of the 16 spectral regions is being considered. Given $\mathcal{C}_i$, the overall capacity of the image $\mathcal{C}_{tot}$ can be easily obtained by letting

$$\mathcal{C}_{tot} = \sum_{i=1}^{16} n_i \mathcal{C}_i,$$

where n_i is the number of coefficient belonging to the i-th sub-region. A similar analysis was performed for the DFT case, the main difference consisting in the spectral region the watermark is inserted in (figure 10b).

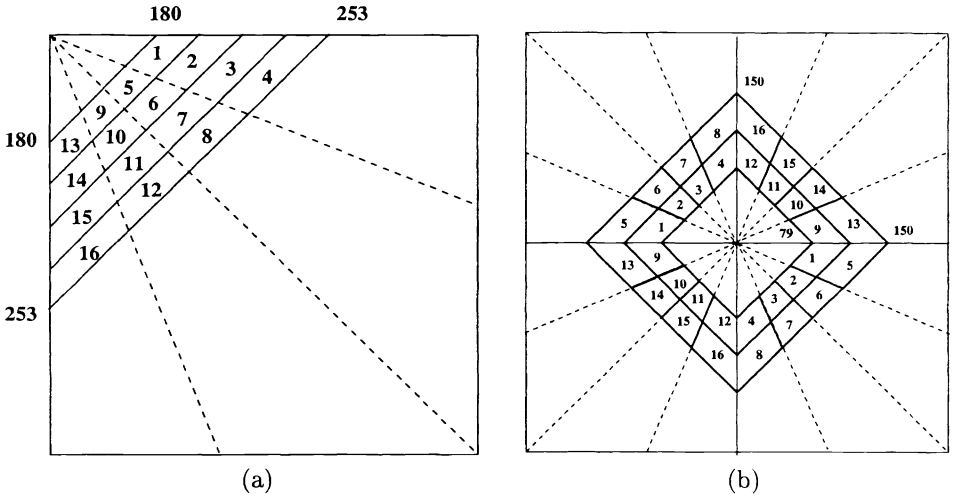

Figure 10. The marked area of the frequency spectrum has been divided into 16 zones for the statistical estimation of the coefficients pdf: (a) DCT spectrum, (b) magnitude of DFT spectrum. Note that in part (b) the regions are duplicated to account for the simmetry properties of the magnitude of the DFT spectrum.

In tables 1 and 2, the number of coefficients belonging to each of the 16 sub-regions displayed in figure 10 is given. Note that the number of watermarked coefficients is nearly the same for the DCT and DFT cases: 16021 in the former case, 16488 in the latter. Note also that the range of watermarked frequencies in the two cases is practically equivalent, even if it is not exactly the same, due to the different meaning of DCT coefficients and the magnitude of DFT samples. As a matter of fact, DCT samples also bear phase information, hence, for a given image size, the number of DCT coefficients is larger than the number of different DFT magnitude samples. The capacity of DCT and DFT samples for the standard Lena image is reported in tables 3 and 4. In the same tables the estimated values of the pdf parameters (ν, σ) and (α, β) are reported for sake of completeness. Finally, table 5 gives the overall watermark-channel capacity for some standard images. In all cases γ was set to 0.2.

6. CONCLUSIONS

The evaluation of the number of bits that can be hidden within a digital image by means of watermarking techniques operating in the frequency domain has been addressed. To this aim the watermarking embedding and retrieval processes have been casted into the classical framework of digital communications through a noisy channel (the watermark-channel). A numerical procedure to evaluate the capacity C_W of the watermark-channel has then been proposed and used to estimate the number of bits which can be reliably hidden into a piece of data of given size. Among the main insights that can be got on the basis of the analysis we carried out, the dependence of C_W on the image energy, i.e. the variance of DCT (DFT) coefficients, and the watermark strength play a major role in the analysis, the design and the evaluation of a watermarking algorithm.

Future research will focus on the extension of the above analysis to spatial and hybrid watermarking algorithms and on the evaluation of the impact that the constraints on watermark invisibility have on C_W. Besides, proper channel models have to be developed to take into account attacks, since attacks appear to be the most important limitation to the reliable concealment and retrieval of information within digital images.

7. ACKNOWLEDGEMENTS

This work was partially supported by the Italian MURST (Ministry of the University and the Scientific and Technological Research).

zone	n_i	zone	n_i	zone	n_i	zone	n_i
1	1056	2	1097	3	1193	4	1362
5	735	6	766	7	832	8	951
9	744	10	775	11	841	12	961
13	1056	14	1097	15	1193	16	1362

Table 1. Number of DCT coefficients belonging to the 16 sub-regions the marked area of the DCT spectrum has been split into.

zone	n_i	zone	n_i	zone	n_i	zone	n_i
1,9	801	2,10	853	3,11	844	4,12	862
5,13	1179	6,14	1235	7,15	1226	8,16	1244

Table 2. Number of DFT magnitude samples contained in each watermarked sub-region of the DFT magnitude spectrum.

zone	σ	ν	$\mathcal{C}/coeff.$	zone	σ	ν	$\mathcal{C}/coeff.$
1	0.4616	1.9469	5.1713	9	0.4656	1.9661	5.2145
2	0.4180	1.9775	5.2398	10	0.3700	1.9748	5.2331
3	0.3565	1.8170	4.8737	11	0.3711	1.7762	4.7793
4	0.2996	1.8320	4.9075	12	0.3150	1.8102	4.8573
5	0.5912	2.0349	5.3686	13	0.2400	1.4926	4.0984
6	0.4881	2.0014	5.2937	14	0.1968	1.7706	4.7610
7	0.4354	2.0612	5.4260	15	0.1734	1.5091	4.1351
8	0.4003	1.7571	4.7349	16	0.1563	1.5582	4.2529

Table 3. Estimated values of σ and ν for image *Lenna* in the 16 zones and relative channel capacity ($\times 10^{-2}$) per coefficient.

zone	β	α	$\mathcal{C}/coeff.$	zone	β	α	$\mathcal{C}/coeff.$
1	1.8744	0.0594	9.2269	9	2.0355	0.0580	10.6864
2	1.8093	0.0710	8.6585	10	2.1208	0.0585	11.4876
3	1.8339	0.0616	8.8713	11	1.9085	0.0411	9.5293
4	1.7944	0.0290	8.5277	12	1.7912	0.0270	8.4999
5	1.9160	0.0321	9.5950	13	1.8808	0.0371	9.2823
6	1.8648	0.0467	9.1418	14	1.8477	0.0345	8.9910
7	1.6483	0.0370	7.3072	15	1.9160	0.0265	9.5937
8	1.8595	0.0167	9.0872	16	1.9395	0.0175	9.7992

Table 4. Estimated values of α and β for the standard image *Lenna* in the 16 zones, and relative channel capacity ($\times 10^{-2}$) per coefficient

Image	$C_{tot}/image - DCT$	$C_{tot}/image - DFT$
airplane	695	1576
boat	798	1389
bridge	822	1586
harbor	747	1403
lenna	776	1522
peppers	689	1526

Table 5. Watermark-channel capacity for six standard images. Both DCT- and DFT-domain capacities are given.

REFERENCES

1. M. D. Swanson, M. Kobayashi, and A. H. Tewfik, "Multimedia data-embedding and watermarking technologies," *Proceedings of the IEEE* **86**, pp. 1064–1087, June 1998.
2. S. Craver, N. Memon, B. L. Yeo, and M. M. Yeung, "Resolving rightful ownership with invisible watermarking techniques: limitations, attacks and implications," *IEEE Journal of Selected Areas in Communications* **4**, pp. 573–586, May 1998.
3. A. Piva, M. Barni, F. Bartolini, and V. Cappellini, "Application-driven requirements for digital watermarking technology," in *Proc. EMMSEC'98, European Multimedia Microprocessor System and Electronic Commerce Conference and Exhibition*, pp. 513–520, (Bordeaux, France), September, 28-30 1998.
4. W. Zeng and B. Liu, "On resolving rightful ownership of digital images by invisible watermarks," in *Proc. ICIP97, IEEE Int. Conf. on Image Processing*, pp. 552–555, (Santa Barbara, California), October 1997.
5. J. R. Smith and B. O. Comiskey, "Modulation and information hiding in images," in *Proc. of First Int. Workshop on Information Hiding, Lecture Notes in Computer Science*, vol. 1174, pp. 207–226, 1996.
6. S. D. Servetto, C. I. Podilchuk, and K. Ramchandran, "Capacity issues in digital image watermarking," in *Proc. ICIP'98, IEEE Int. Conf. on Image Processing*, pp. I:445–449, (Chicago, Illinois, USA), 4-7 October 1998.
7. C. E. Shannon, "A mathematical theory of communications," *Bell Syst. Techn. Journ.* **27**, pp. 623–656, October 1948.
8. I. J. Cox, J. Kilian, T. Leighton, and T. Shamoon, "Secure spread spectrum watermarking for multimedia," *IEEE Trans. Image Processing* **6**, pp. 1673–1687, December 1997.
9. M. Barni, F. Bartolini, V. Cappellini, and A. Piva, "A DCT-domain system for robust image watermarking," *Signal Processing* **66**, pp. 357–372, May 1998.
10. M. Barni, F. Bartolini, and A. Piva, "Copyright protection of digital images by means of frequency domain watermaking," in *Mathematics of Data/Image Coding, Compression, and Encryption, Mark S. Schmalz ed., Proceedings of SPIE, vol. 3456*, pp. 25–35, (S.Diego, CA), July, 21-22 1998.
11. J. J. K. Ó. Ruanaidh and T. Pun, "Rotation, scale and translation invariant digital image watermarking," in *Proc. ICIP'97, IEEE Int. Conf. on Image Processing*, vol. I, pp. 536–539, (Santa Barbara, CA), 26-29 October 1997.
12. T. Kalker, J. P. Linnartz, G. Depovere, and M. Maes, "On the reliability of detecting electronic watermarks in digital images," in *Proceedings of EUSIPCO'98, Ninth European Signal Processing Conference*, pp. 13–16, (Rodos, Greece), September, 8-11 1998.
13. R. G. Gallager, *Information Theory and Reliable Communication*, Wiley, New York, 1968.
14. F. Müller, "Distribution shape of two-dimensional DCT coefficients of natural images," *Electronic Letters* **29**, pp. 1935–1936, October 1993.
15. R. L. Joshi and T. R. Fischer, "Comparison of Generalized Gaussian and Laplacian modeling in DCT image coding," *IEEE Signal Processing Letters* **2**, pp. 81–82, May 1995.
16. M. Barni, F. Bartolini, A. Piva, and F. Rigacci, "Statistical modelling of full frame dct coefficients," in *Proceedings of EUSIPCO'98, Ninth European Signal Processing Conference*, pp. 1513–1516, (Rodos, Greece), September, 8-11 1998.